Macroporous polymer nanocomposites synthesised from high internal phase emulsion templates stabilised by reduced graphene oxide

Ling L. Ching Wong [a,b,1], Suelen Barg [c,1], Angelika Menner [b], Paula do Vale Pereira [c], Goki Eda [d], Manish Chowalla [e], Eduardo Saiz [c], Alexander Bismarck [a,b,*]

[a] Polymer & Composite Engineering (PaCE) Group, Department of Chemical Engineering, Imperial College London, South Kensington Campus, London SW7 2AZ, UK
[b] Polymer & Composite Engineering (PaCE) Group, Institute of Materials Chemistry & Research, Faculty of Chemistry, University of Vienna, Währingerstr. 42, A-1090 Vienna, Austria
[c] Department of Materials, Centre for Advanced Structural Ceramics (CASC), Imperial College London, South Kensington Campus, London SW7 2AZ, UK
[d] Physics Department, National University of Singapore, Singapore 117542, Singapore
[e] Department of Materials Science and Engineering, The State University of New Jersey, NJ 08854, USA

1. Introduction

Graphene, a two-dimensional (2D) monolayer of sp^2 carbon atoms packed into a honeycomb lattice, has attracted much scientific attention in recent years due to its properties including high elasticity, stiffness, electron mobility and thermal conductivity [1–6]. However, synthesising pure graphene using methods such as chemical vapour deposition is impractical considering the large volumes of material required to produce viable, three-dimensional (3D) structures and graphene-based nanocomposites. To address this demand, graphite is chemically exfoliated, producing graphene oxide (GO) in bulk quantities [7,8]. Due to the presence of hydrophilic dissociable functional groups on the basal plane edges and the hydrophobic unoxidised graphitic nano-islands within the basal plane, GO exhibits hydrophilic and hydrophobic regions in an edge to centre configuration [9–11]. As a result, GO has been shown to adsorb at the air/water and oil/water interface and is able to stabilise o/w emulsions [10–14]. In some studies, GO stabilised w/o emulsion droplets, which yielded hollow GO spheres upon drying [15,16]. However, since there are no mobilised electrons in the sp^3 C–O bonds found in GO, it is electrically insulating, limiting its use in certain applications. Chemical or thermal reduction effectively restores some of the C–C sp^2 bonds lost when graphene is oxidised to GO [6,17,18]. The resulting semiconductor material,

* Corresponding author. Polymer & Composite Engineering (PaCE) Group, Department of Chemical Engineering, Imperial College London, South Kensington Campus, London SW7 2AZ, UK.
E-mail addresses: alexander.bismarck@univie.ac.at, a.bismarck@imperial.ac.uk (A. Bismarck).
[1] These authors contributed equally to this work.

known as reduced GO (rGO), was reported to posses similar electrical, thermal and mechanical properties as pristine graphene [17,19]. In addition, reduction removes most of the oxygen-containing functional groups in GO [8,19]. This maintains the ability of rGO to still adsorb at oil–water interfaces but increases the affinity of rGO for hydrophobic solvents over water [20]. This is one of the properties that make rGO a suitable candidate for the manufacture of conductive macroporous polymer nanocomposites via water-in-oil (w/o) emulsion templating.

Numerous attempts have been made to incorporate graphene, GO and rGO into functional materials. This motivation to translate 2D graphene, GO and rGO into 3D structures is driven by the favourable properties that graphene, GO and rGO impart to the final material. For example, the use of graphene as a nanofiller imparts electrical conductivity to the resulting dense polymer nanocomposites [4,21], highly sought after for numerous industrial applications [22–26]. Graphene and GO when used as nanofillers in polymer composite films have shown improved mechanical properties [27,28]. Recently, the spotlight has shifted to the production of alternative 3D GO-based materials such as hollow GO spheres by drying GO-stabilised w/o emulsions [15] or GO-polystyrene beads by polymerising o/w emulsion templates stabilised by GO [12]. There has also been considerable interest in the production of graphene, GO and rGO based foams for various applications ranging from gas sensors, oil adsorbents to biosensor devices [29–34]. However, the production of rGO-based macroporous polymer nanocomposites by polymerising w/o emulsions (containing monomers in the oil phase) stabilised solely by rGO has yet to be reported. We are proposing emulsion templating as an alternative, viable method to translate 2D rGO into 3D conductive macroporous materials.

Emulsion templating is a versatile method to synthesise macroporous polymers with tuneable pore structures [35,36]. In conventional emulsion templating, an aqueous phase, often an electrolyte, is emulsified with the oil phase (consisting of monomers and crosslinkers, such as styrene and divinylbenzene, a suitable initiator and emulsifier) to produce water-in-oil (w/o) emulsion templates. Individually dispersed water droplets act as templates for the final macroporous structure at the gel point of the polymerisation [35,37], hence the term emulsion templating. W/o emulsions with an internal phase volume greater than 74 vol.% are defined as high internal phase (ratio) emulsions (HIPEs) [38]. After HIPEs are polymerised, purified and dried to remove the water phase, macroporous polymers are obtained which are known as poly(merized)HIPEs or polyHIPEs. PolyHIPEs are lightweight, have a low foam density and low thermal conductivity. Since emulsion templates are liquid, they can be injected [39], moulded [40] or cast into membranes [41]. Depending on the emulsifier used, the morphology of the synthesised macroporous polymers differs. PolyHIPEs synthesised from surfactant stabilised HIPEs are recognisable by their high degree of pore interconnectivity. Pores have diameters ranging from 5 to 100 μm with interconnecting pore throats that have diameters ranging from 20 to 50% of the pore size, connecting each individual pore [42]. The high surfactant concentration used to produce HIPEs is a major cost factor [43] and if not removed properly from resultant polyHIPEs, has been shown to affect the final physical properties of polyHIPEs [44]. Particles can also stabilise emulsions by adsorption at liquid–liquid interfaces forming what is known as particle-stabilised or Pickering emulsions [45]. They tend to adsorb almost irreversibly (with very high associated energy) at oil–water interfaces resulting in very stable emulsions [46]. A range of modified inorganic and organic particles including silica, titania, carbon nanotubes (CNT) and nanocellulose have been used to prepare particle-stabilised HIPEs or Pickering HIPEs [47–49]. Polymerisation of particle-stabilised HIPEs results in poly-Pickering-HIPEs, which are closed-cell and have higher mechanical properties due to the reinforcing effect of the particulate emulsifier [50]. Due to these properties, poly-Pickering HIPEs have potential applications, ranging from thermal or acoustic insulation, packaging to speciality applications in composites. Poly-Pickering-HIPEs could potentially complete with commonly used foams such as high performance closed cell polymer foams, such as Rohacell® and Divinycell, which are being used in sandwich composite structures.

In this work rGO is produced by the controlled thermal reduction of GO. The ζ-potentials of GO and rGO are first measured as a function of pH and compared with one another to verify the suitability of rGO to stabilise w/o emulsions. Subsequently, rGO was used to stabilise w/o HIPEs containing the monomers styrene and divinylbenzene in the oil phase. After polymerisation and purification, highly porous, closed-cell rGO-poly(St-co-DVB)HIPEs were produced. The pore structure of these macroporous polymer nanocomposites was determined and the influence of the rGO content on its mechanical and electrical properties characterised.

2. Experimental section

2.1. Materials

Natural graphite, divinylbenzene (DVB), styrene (St), oleic acid, chloroform, methanol, calcium chloride dihydrate and acetone were purchased from Sigma Aldrich (Kent, UK) and used without further purification. α,α′-azoisobutyronitrile (AIBN) was purchased from Camida, (Tipperary, Ireland). The nonionic polymeric surfactant Hypermer 2296 was kindly supplied by Uniqema (Wirral, UK) and spherical hydrophilic titania particles (P25) were provided by DEGUSSA AG (Frankfurt, Germany).

2.2. Preparation of modified titania particles

Hydrophilic titania particles were hydrophobised by the physical adsorption of oleic acid using a mixture of oleic acid and chloroform following a procedure described elsewhere [51]. The titania particles were then washed with chloroform to remove the excess oleic acid, centrifuged and vacuum dried at 120 °C for 24 h. Thermogravimetric analysis was used to determine the oleic acid content, which was found to be 3.5 ± 1 wt.%.

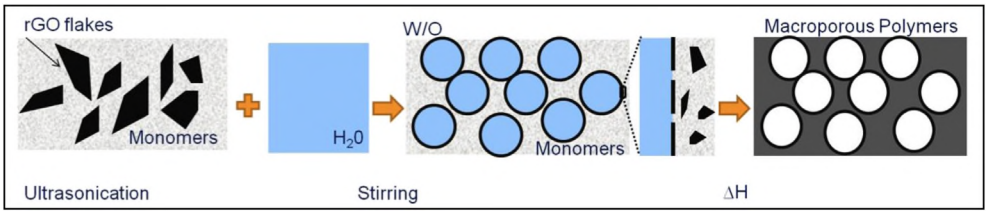

Fig. 1. Schematic illustrating the fabrication procedure of macroporous polymer nanocomposites.

2.3. Synthesis of rGO particles

Firstly, GO suspensions were produced by exfoliating graphite using a modified Hummers method [52]. The resulting suspension was transferred into 85 ml polycarbonate centrifuge tubes (Nalge Nunc International Corp. EDI) and centrifuged at 10,000 rpm followed by the removal of the supernatant and addition of deionised water. This process was repeated until the pH of the suspension was greater than 4.5. Non-exfoliated particles were then removed by centrifugation at 3000 rpm. The efficiency of the process was monitored using optical microscopy (Axio Imager 1, Carl Zeiss, UK). GO particles were first obtained by freeze-drying GO suspensions (Freezone 4.5, Labconco Corporation, USA) for 48 h below 0.1 mbar. 60–90 mg of freeze-dried GO particles were then placed in an alumina crucible forming a compact layer. The crucible was inserted in the middle of a quartz tube, which was then placed into the tubular oven (Carbolite Furnaces, UK), heated to 800 °C and held for 5 h in a 10%H_2/90%Ar atmosphere to produce rGO particles.

2.4. Preparation of rGO-poly(St-co-DVB)HIPEs or macroporous polymer nanocomposites

The general methodology developed for the fabrication of rGO-poly(St-co-DVB)HIPEs is illustrated in Fig. 1.

rGO particles at concentrations ranging from 0.1 to 5 mg/ml with respect to organic phase were dispersed in a 1:1 (by volume) mixture of styrene and divinylbenzene (St:DVB) in an ice bath using an ultrasonic tip (IKA U-50 Ultrasonic Processor, IKA GmbH, Germany) for up to an hour to remove any visible aggregates. 25 mg/ml oleic acid modified titania was dispersed in the same 1:1 (by volume) mixture of St:DVB using a homogeniser (Kinematica Luzern, CH) at 15,000 rpm for 10 min (Control 1) while 200 mg/ml of the nonionic polymeric surfactant Hypermer 2296 was dissolved in the same monomer mixture by shaking (Control 2). The free-radical initiator α,α′-azoisobutyronitrile (1 mol.%) was added to all the freshly prepared suspensions. This was followed by the slow, dropwise addition of 75 vol.% with respect to total emulsion volume of 5 g/L $CaCl_2$ $2H_2O$ aqueous solution under continuous stirring using a vortex mixer (Genie 2™, Scientific Industries, USA). In order to have porosities in the same range as those of the poly-Pickering-HIPEs produced by polymerisation of rGO stabilised HIPEs, note that 80 vol.% of the same aqueous phase was used to prepare the controls. Finally the stirring rate was increased until an emulsion was formed. In the case of the two control samples, the aqueous solutions were added using experimental setups reported previously [51,53]. All emulsions were then transferred into 15 ml polypropylene SuperClear™ centrifuge tubes, which were sealed and placed for polymerisation of the HIPEs in a convection oven at 70 °C for 24 h to obtain macroporous poly(St-co-DVB). The macroporous polymer nanocomposites were removed from the centrifuge tubes and dried in a vacuum oven at 110 °C until a constant weight was achieved; a temperature slightly above the boiling point of water was chosen in order to facilitate the removal of moisture from the predominantly closed cell macroporous polymers.

2.5. Electrophoretic mobility of GO and rGO particles

Electrophoretic mobility measurements were carried out using a ZetaPALS (Zeta Potential and Particle Size Analyzer, Brookhaven Instruments, Holsville, NY, USA). GO and rGO were dispersed in a 1 mM KCl electrolyte (0.03 mg/ml) using an ultrasonic tip and the pH adjusted (pH 3–10) by the addition of 0.1 and 0.05 M HCl or KOH, respectively. GO was well dispersed after approximately 10 s of ultrasonication whilst for rGO, due to its hydrophobic nature, it took a considerably longer time, 10 min, to disperse before the solutions appeared to be clear. All dispersions were measured fresh after preparation to minimise the effects of aggregation. ζ-potential was calculated from the measured electrophoretic mobility μ_e using the Henry equation with the Smoluchowski approximation [54] (Equation (1)):

$$\mu_e = e\frac{\zeta}{\eta} \tag{1}$$

where e and η are the dielectric constant and the viscosity of the suspending liquid, in this case, the aqueous electrolyte.

2.6. Characterization of rGO emulsion templated nanocomposite macroporous polymers

Scanning Electron Microscopy (LEO Gemini 1525 and JEOL JSM 5610 LV) was used for the microstructural analysis of uncoated macroporous polymer nanocomposites. The samples were fractured to reveal the internal surfaces and washed with deionised water. The samples were then stuck on carbon adhesive stickers (Agar Scientific, UK) attached to SEM specimen stubs (Agar Scientific, UK) and vacuum dried at 110 °C until the weight was constant. Pore sizes were measured using the linear intercept method using the software Linear Intercept (TU Darmstadt, Germany). The software measures a minimum of 150 pores for each sample and the cumulative pore size distribution curves were plotted. From these curves, the characteristic pore sizes of d_{10}, d_{50} and d_{90}, corresponding to the pore diameter at the cumulative percentage size of 10, 50 and 90%, respectively, were extracted.

The skeletal density ρ_s of the nanocomposites was measured using He displacement pycnometry (Accupyc 1330, Micrometrics Ltd., Dunstable, UK) by placing ~20 mg of powdered macroporous polymer nanocomposites into a vessel of known volume. The envelope density ρ_e was calculated from the measured mass m and volume V of cubes of macroporous polymer nanocomposites ($\rho_e = m/V$). The percentage porosity P is:

$$P = \left(1 - \frac{\rho_e}{\rho_s} \times 100\%\right) \tag{2}$$

Dynamic mechanical properties of the macroporous polymer nanocomposites were investigated using dynamic mechanical analysis (Perkin Elmer DMA 8000 MA, USA). Specimens were cut into 5 × 5 × 5 mm^3 cubes and a controlled strain was applied at a rate of approximately 0.2 s^{-1} and a constant frequency of 1 Hz while keeping the temperature constant at 30 °C. The compressive stress required to deform the materials to a specific strain was used to calculate the storage modulus.

Uniaxial compression tests were performed (Lloyds EZ50, Lloyds Instruments Ltd., Fareham, UK) at room temperature following the industrial standard BS ISO 844. The samples were cut into cylinders with a diameter to height ratio of approximately 1 using a bench saw (Titan SF8R Screwfix, UK). These cylinders were then machined until the edges were parallel. The bottom and top part of each sample was filled with a thin layer of liquid paraffin wax at 60 °C and connected to a glass slide. This preparation method ensured that the load was transferred evenly onto the macroporous polymer nanocomposites during compression. The compression platens were sprayed with Teflon (Rocol, Swllington, Leeds, UK) prior to each measurement and each specimen was loaded at a crosshead speed of 1 mm/min until a maximum displacement of about 50% was reached or the specimen fractured abruptly, whichever occurred first. The elastic modulus is obtained from the slope of the linear portion of the stress–strain curve. The crush strength was

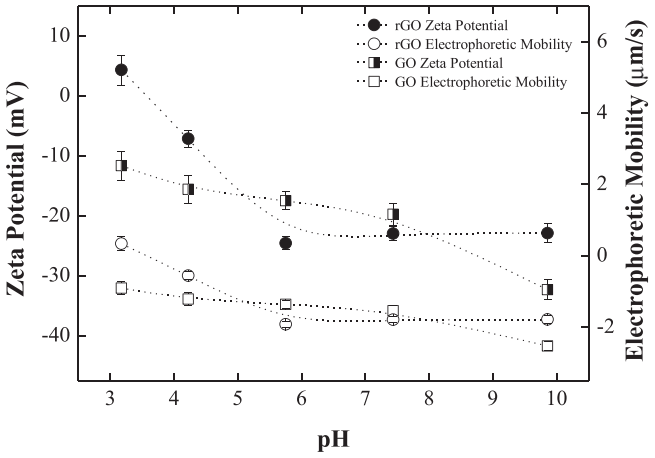

Fig. 2. ζ-potential and electrophoretic mobility of a dispersion of 0.03 mg/ml GO and rGO in an aqueous 1 mM KCl supporting electrolyte as a function of pH.

taken as the maximum stress at the end of the initial linear elastic region.

To measure electrical conductivity, macroporous polymer nanocomposites were cut into disks of 12.5 mm diameter and 5 mm thickness and the upper and bottom surfaces coated with silver paint (Ernest F. Fullam Inc., Redding, CA, USA). The electrical resistance R of the macroporous polymer nanocomposites was measured using the 2-point method with a digital multimeter (Kusam-Meco Digital Multimeter KM320). The resistivity ρ was calculated taking into account the cross sectional area A and the sample thickness t as follows (Equation (3)). The conductivity was then calculated as the inverse of resistivity.

$$\rho = R \times \frac{A}{t} \tag{3}$$

3. Results and discussion

3.1. Electrophoretic mobility and ζ-potential of GO and rGO dispersions

GO and rGO (0.03 mg/ml) were dispersed in electrolyte solutions (1 mM KCl) of different pH. Dissociation of surface functional groups according to their pK_a values and adsorption of H_3O^+ or OH^- from the aqueous electrolyte solutions resulted in the formation of a net charge on the surface of GO and rGO, which was measured as the electrophoretic mobility. The corresponding ζ-potentials were then calculated and displayed in Fig. 2 as function of pH. In general, the ζ-potential was observed to decrease with increasing pH for both GO and rGO. This suggests the presence of Brønsted acid surface groups, such as carboxylic acids, on both GO and rGO, which dissociate in contact with the aqueous electrolyte and are fully deprotonated at high pH [10,55]. While the ζ-potential for GO continued to decrease from −17 mV to −33 mV between pH 6 to 10, the ζ-potential for rGO remained constant at approximately −23 mV in this pH range. This suggests that rGO contains a smaller number of dissociable acidic surface groups compared to GO, which were fully deprotonated at a lower pH, also in comparison to GO. The isoelectric point (iep), the point at which ζ = 0 mV, is determined by the concentrations and relative pK_a

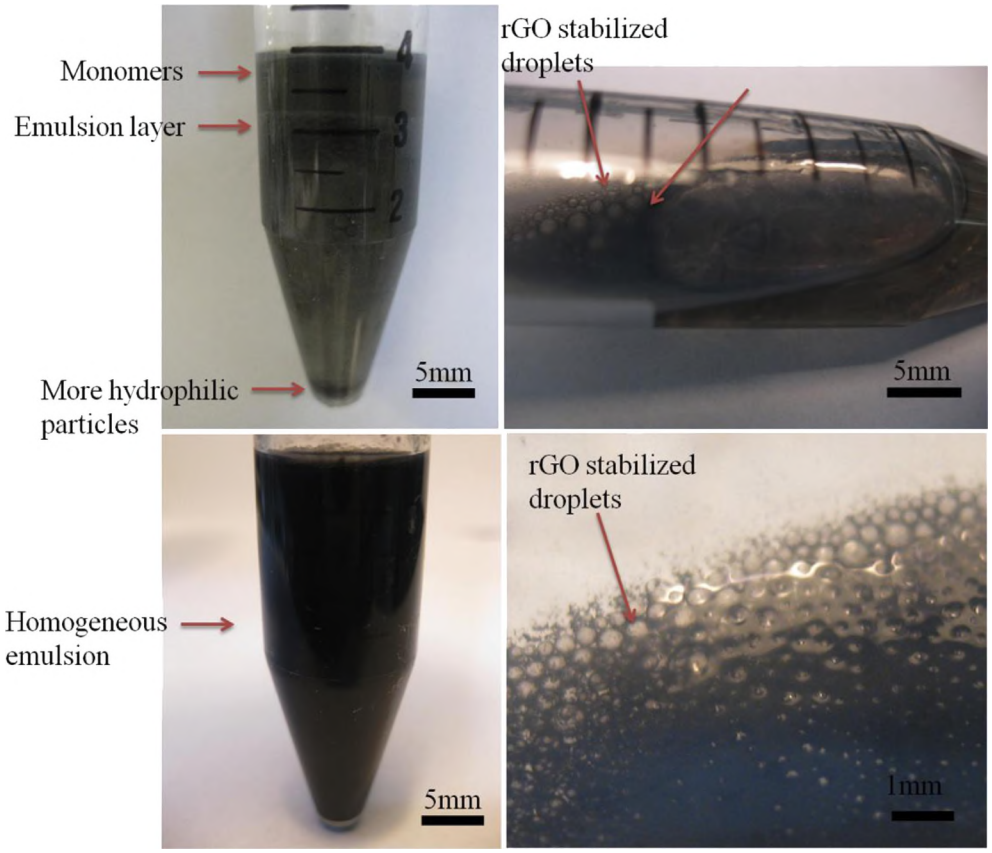

Fig. 3. Comparing w/o HIPEs stabilised by two rGO concentrations. The photographs on top show a HIPE stabilised by 0.1 mg/ml rGO separating into oil and water layers within 30 s after preparation due to rapid droplet coalescence. Photographs on the bottom row show a HIPE stabilised by 1.2 mg/ml rGO, which remained stable for at least 30 days on the bench. This behaviour was representative for all other HIPEs stabilised by rGO concentrations exceeding 0.2 mg/ml prepared in this series.

Table 1
Summary of porosity and densities of rGO-poly(St-co-DVB)HIPEs, control samples 1 and 2.

Specimen name	Emulsifier	Emulsifier concentration (mg/ml)[a]	Porosity (%)	Skeletal density (g/cm^3)	Envelope density (g/cm^3)
rGO 0.2[b]	rGO	0.2	86.0 ± 0.3	1.081 ± 0.007	0.1513 ± 0.0005
rGO 0.4	rGO	0.4	85.5 ± 0.2	1.076 ± 0.007	0.1568 ± 0.0005
rGO 0.8	rGO	0.8	83.8 ± 0.3	1.073 ± 0.003	0.1738 ± 0.0002
rGO 1.2	rGO	1.2	81.7 ± 0.3	1.080 ± 0.009	0.1967 ± 0.0004
rGO 1.6	rGO	1.6	82.7 ± 0.3	1.080 ± 0.007	0.1866 ± 0.0002
rGO 2	rGO	2	81.7 ± 0.2	1.073 ± 0.004	0.1976 ± 0.0007
rGO 2.4	rGO	2.4	83.0 ± 0.3	1.083 ± 0.007	0.1823 ± 0.0007
rGO 5	rGO	5	82.0 ± 0.3	1.081 ± 0.004	0.1946 ± 0.0004
'Control 1'	titania	25	85 ± 2	1.12 ± 0.02	0.246 ± 0.010
'Control 2'	Hypermer 2296	200	84 ± 1	1.10 ± 0.03	0.180 ± 0.010

[a] Calculated with respect to monomer volume, which was 25 vol.% for rGO and 20 vol.% for controls.
[b] rGO 0.2 refers to rGO-poly(St-co-DVB)HIPEs prepared from emulsion templates stabilised by 0.2 mg/ml rGO, rGO 0.4 refers to rGO-poly(St-co-DVB)HIPEs prepared from emulsion templates stabilised by 0.4 mg/ml rGO and so on.

values of all functional groups present on the surface of GO and rGO. For GO, the iep was extrapolated to be slightly less than pH 1 while for rGO it was found to be at pH 3.6, demonstrating the more acidic nature of the GO surface compared to rGO once again. Our observations are in line with earlier reports on the removal of hydrophilic −COOH and −C═O groups from the surface of GO during thermal reduction, therefore making them more hydrophobic in nature [19,56]. This difference in surface composition and nature of the functional groups does explain why it is much easier to disperse GO in the aqueous electrolyte compared to rGO.

3.2. Characterisation of macroporous polymer nanocomposites

The rGO concentration required to emulsify 75 vol.% water in the organic phase was found to be as low as 0.1 mg/ml (with respect to the organic phase), which was the lowest rGO concentration used in this study. HIPEs stabilised by this rGO concentration were initially homogeneous but underwent fast droplet coalescence and consequently phase separation before polymerisation could be completed. This was evident from the separate 'layers' observed when the emulsion was left on the bench at room temperature for about 30 s after preparation (Fig. 3(a) left). Thus, it was impossible to produce polyHIPE monoliths from this HIPE template required for further characterisation. A close up photo of the emulsion revealed the extent of droplet coalescence (Fig. 3(a) right). In contrast to HIPEs stabilised by 0.1 mg/ml rGO, HIPEs stabilised by 0.2 mg/ml rGO dispersions remained stable on the bench at room temperature and during the course of polymerisation. Once this lower concentration limit of rGO required for HIPE stabilisation was determined, emulsion templates with increasing rGO concentrations (from 0.4 to 5 mg/ml) were prepared to determine its influence on the microstructure and properties of the resultant macroporous polymer nanocomposites.

The photo of an emulsion stabilised by 1.2 mg/ml of rGO is shown in Fig. 3(b). A close-up photo shows individual water droplets surrounded by a black-coloured organic phase layer containing rGO (Fig. 3(b) right) in contrast to separate phases previously observed for the HIPEs stabilised with 0.1 mg/ml rGO (Fig. 3(a)).

Polymerising the rGO stabilised HIPE templates followed by washing and drying resulted in high porosity rGO-poly(St-co-DVB) HIPEs. All porosities measured for rGO-poly(St-co-DVB)HIPEs were higher than the internal phase volume fraction used to prepare the emulsions (75 vol.%). This was attributed to a combination of the inevitable loss of organic phase by evaporation during the 1 h long dispersion and transfer of the viscous continuous phase between containers (approximately 0.5 ml lost for every 2 ml of organic phase) and in some cases also because of droplet sedimentation occurring in the HIPEs. Skeletal densities of the rGO-poly(St-co-DVB)HIPEs (Table 1) were constant within error since the very small concentration of rGO used to stabilise the HIPEs did not significantly affect the overall density of the macroporous polymer nanocomposites. rGO 0.2 (or macroporous polymer nanocomposites synthesised from emulsion templates stabilised by 0.2 mg/ml of rGO) had the lowest envelope density and consequently the highest porosity at 86% as its HIPE template sedimented partially during polymerisation. The droplet sedimentation caused some separation of the organic phase from the emulsion, which resulted in an approximately 2−3 mm thick layer of dense polymer on top of the porous material, which was removed. Porosity decreased from 86% to 84% as the rGO concentration used to stabilise HIPEs was increased to 0.8 mg/ml. The higher concentration of rGO stabilised more w/o interface, reducing the

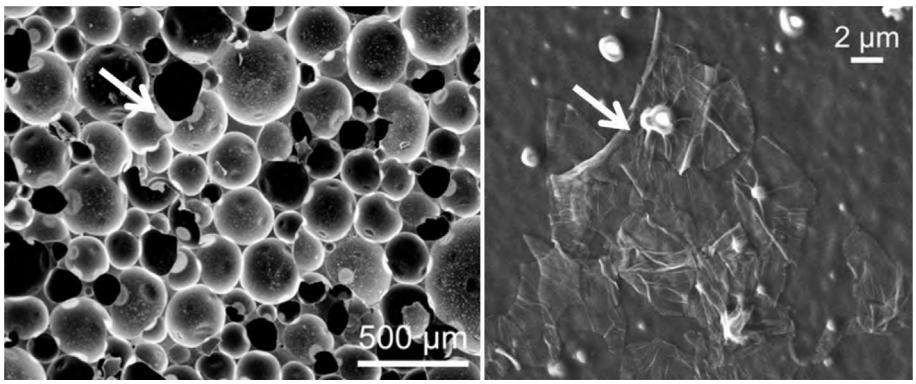

Fig. 4. SEM of a rGO-poly(St-co-DVB)HIPE synthesised by the polymerisation of a 75 vol.% w/o HIPE stabilised by 1.2 mg/ml rGO (left). rGO particles covering the internal surface of a pore in a rGO-poly(St-co-DVB)HIPE are indicated with an arrow (right).

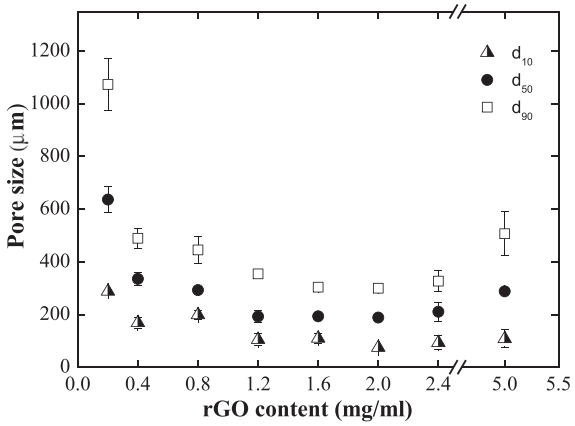

Fig. 5. The characteristic pore sizes d_{10}, d_{50} and d_{90} of rGO-poly(St-co-DVB)HIPEs as a function of rGO concentration used to stabilise the HIPE templates.

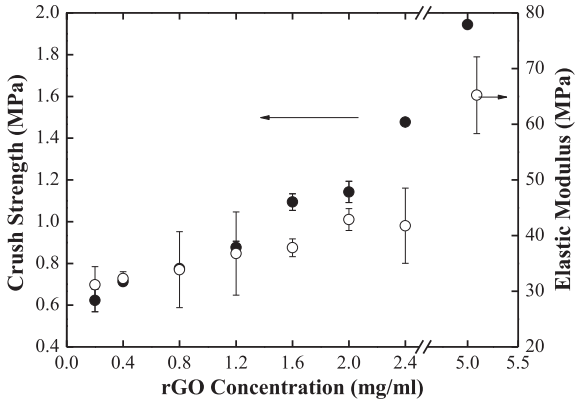

Fig. 6. Crush strengths (open dots) and elastic moduli (black filled dots) of rGO-poly(St-co-DVB)HIPEs as function of rGO concentration.

effect of droplet sedimentation during polymerisation. The dense polymer layer found on top of the macroporous structure decreased to about 1–2 mm compared to rGO 0.2, resulting in a lower porosity measured for rGO 0.8 compared to rGO 0.2. Porosity continued to decrease to 82% for rGO 1.2 and remained constant from rGO 1.2 to rGO 5; no further droplet sedimentation was observed and, therefore, no dense polymer layer was formed for rGO 1.2 to rGO 5 during polymerisation.

High resolution SEM was used to elucidate the pore structure of rGO-poly(St-co-DVB)HIPEs. A representative image of rGO 1.2 is shown in Fig. 4. The rGO-poly(St-co-DVB)HIPEs have a closed-cell pore structure that is typical for conventional, poly-Pickering-HIPEs prepared by polymerisation of particle stabilised emulsion templates [43,57]. Higher magnification of the pore walls of a rGO-poly(St-co-DVB)HIPE sample revealed rGO particles covering a section of a pore (Fig. 4, right). Since the emulsion structure is 'frozen' at the gel point of polymerisation, it indicates that rGO did segregate to the w/o interface. The ultrasonication process used to prepare the organic phase for emulsification was, therefore, effective in dispersing rGO particles as they appeared intact and no large agglomerates were seen at the former o/w interface.

The cumulative pore size distributions of the rGO-poly(St-co-DVB)HIPEs were obtained by SEM image analysis. From this analysis, the characteristic d10, d50 and d90 pore sizes were determined and displayed as a function of rGO concentration used to stabilise the HIPE templates in Fig. 5. Additional SEM images of the microstructure of rGO-poly(St-co-DVB)HIPEs with different rGO content can be seen in the supplementary information, Fig. S1. rGO 0.2 possessed the largest pores with a d_{50} pore size of 636 μm, which means that 50% of the pore sizes are identical or smaller than this value. Also rGO 0.2 has the broadest pore size distribution, which can be determined from the range between d_{10} and d_{90} values. The pore size distributions became narrower and the d_{50} pore size smaller with increasing rGO concentration as more rGO was available to stabilise smaller droplets. The smallest d_{50} pore size of 192 μm was observed for rGO 1.2. The pore size remained constant as for poly-Pickering-HIPEs prepared by the polymerisation of HIPEs stabilised with increasing rGO concentrations until 2 mg/ml (rGO 2). When the rGO concentration in HIPEs was increased further to 5 mg/ml (rGO 5), the pore size distribution became broader again. At concentrations as high as 2.4–5 mg/ml, the amount of energy supplied by ultrasonication during the preparation of the organic phase was no longer sufficient to completely disperse rGO in the organic phase. As a result, the particles appeared to agglomerate, reducing their effectiveness to stabilise smaller droplets.

Compression testing at constant strain rate using the Lloyds Universal testing machine and dynamic mechanical analysis (DMA) at constant frequency was used to determine the mechanical properties of the rGO-poly(St-co-DVB)HIPEs. Results from these mechanical tests serve to explain the influence of rGO concentration and pore morphology on the crush strength, elastic and storage moduli of the rGO-poly(St-co-DVB)HIPEs. As control samples, we chose conventional poly-Pickering-HIPEs and polyHIPEs with the same porosity as the rGO macroporous polymer nanocomposites. The controls were prepared by polymerising HIPE templates with an internal aqueous phase volume ratio of 80% in a 1:1 (by volume) mixture of St to DVB stabilised by 25 mg/ml of particulate emulsifier (Control 1) and 200 mg/ml of surfactant (Control 2). Porosities, skeletal and envelope densities of the control samples and rGO-poly(St-co-DVB)HIPE samples are summarised in Table 1.

Compression tests have been conducted at a constant strain rate and the crush strength and the elastic modulus were determined from stress–strain curves. Both, the crush strengths and elastic moduli, increased with increasing rGO concentration as can be seen in Fig. 6. As the rGO dispersed in the polymer matrix increased, the wrinkly and creased rGO particles mechanically interlock with other particles within the polymer matrix in a configuration, which seemingly improved the load transfer of the entire macroporous polymer nanocomposite during compression at constant strain. This resulted an increase in mechanical properties with increasing rGO concentration.

As the concentration of rGO increased from 0.2 mg/ml (rGO 0.2) to 1.2 mg/ml (rGO 1.2) a combination of decreasing porosity (Table 1) in addition to the reinforcing effect of rGO resulted in the increase in the crush strength of the macroporous nanocomposites. Recalling Fig. 5, where the d_{50} pore size plateaued at 190 μm (Fig. 5) and porosity remained constant between rGO 1.2 to rGO 2, the further increase in crush strength between rGO 1.2 to rGO 2 provides evidence of the significant reinforcing effect of rGO in the nanocomposite. rGO 5 had the highest in crush strength when compared to rGO 2 as the pore size distribution broadened (Fig. 5 and Fig. S1) while the porosity remained constant between rGO 2 to rGO 5 (Table 1). Besides the additional reinforcing effect of rGO, the broadly distributed pore sizes (Fig. 5 and Fig. S1) also contributed to the improvement in crush strength observed. It was previously shown that when the porous structure of a polyHIPE consists of a combination of larger and smaller pores at the same porosity, the load transfer mechanism is improved, improving the overall mechanical properties of the porous material [40,58].

Control 1, a poly-Pickering-HIPE synthesised from a w/o-HIPE stabilised by oleic acid modified titania, had a crush strength of

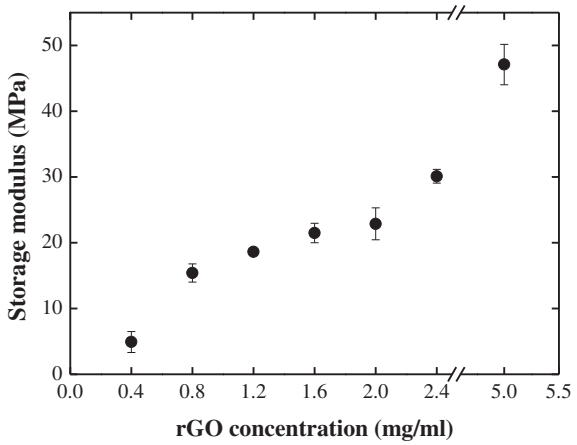

Fig. 7. Storage moduli of rGO-poly(St-co-DVB)HIPEs as function of rGO concentration used to stabilise the respective emulsion templates (with regards to organic phase) obtained from dynamic mechanical analysis.

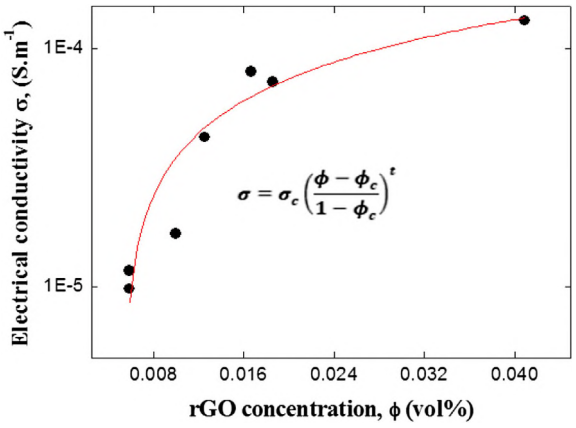

Fig. 8. Electrical conductivity σ of rGO-poly(St-co-DVB)HIPEs as a function of rGO volume fraction Φ (calculated assuming the density of bulk rGO to be 2.2 g/cm^3 [4] and with regards to the total volume of the macroporous polymer nanocomposites including all the emulsifying rGO when calculating the nanofiller volume). The solid line is the best fit of the conductivity equation (inserted equation in Fig. 7) [59] to our data, where σ_c is the conductivity of the filler, Φ_c is the percolation threshold and t percolation exponent. The fitted parameters are: $\Phi_c = 0.005$ vol.%, $\sigma_c = 0.020$ S m^{-1}, $t = 0.7$ (dimensionless).

3.2 ± 0.8 MPa, 65% higher than the maximum measured for rGO 5. This can be explained by the fact that a much higher particulate emulsifier concentration (five times higher) was needed. The particles also acted as reinforcement of the pore walls, in addition to the difference in pore size, both factors contributing to a higher crush strength. However, when compared with rGO 5, the elastic modulus of Control 1 is still 68% lower at 21 ± 3 MPa despite possessing a similar porosity. This is due to the packing as rGO flakes into a network which seems to impart greater stiffness, resulting in a more efficient reinforcement to the polymer foam compared to titania. Control 2, a conventional polyHIPE, obtained by the polymerisation of a HIPE stabilised using 200 mg/ml of a non-ionic polymeric surfactant (Hypermer 2296), had a 55% lower elastic modulus at 29 ± 4 MPa and 23% lower crush strength at 1.5 ± 0.2 MPa compared to that of rGO 5 [58]. The lower mechanical properties of Control 2 are caused by the presence of interconnecting pore throats, which weakened the overall porous structure. As such, rGO particles are not only a more efficient emulsifier at lower concentrations, it did also result in higher elastic moduli and crush strengths when compared to porous materials prepared via conventional emulsion templating using other particle- and surfactant-stabilised emulsions.

Moving on to the storage moduli, obtained from dynamic mechanical measurements under compression at constant frequency, it was generally observed that the storage moduli increased with increasing rGO concentration (Fig. 7). Due to the brittle nature of samples (rGO 0.2) prepared by polymerisation of HIPEs stabilised by 0.2 mg/ml, it was difficult to cut them and determine the storage modulus accurately and so the data were excluded. Doubling the rGO concentration in HIPE templates from 0.4 mg/ml to 0.8 mg/ml resulted in an approximately three-fold increase of the storage modulus. An increase in rGO concentration from 0.8 mg/ml to 5 mg/ml (rGO 0.8 to rGO 5) further increased the storage modulus of the rGO-poly-Pickering-HIPEs a further three-fold. This is a result of a combination of the reinforcing effect of increasing loadings of rGO in the polymer matrix as well as the positive influence of pore size and arrangement (Fig. S1) on the storage modulus. In comparison, both controls 1 and 2 had significantly lower storage moduli; 77% lower at 11 ± 9 MPa for Control 1 and 66% lower at 16 ± 3 MPa for Control 2 compared to the maximum storage modulus measured for the macroporous polymer nanocomposites prepared from rGO stabilised HIPEs (47 ± 3 MPa for rGO 5).

The conductivity of macroporous polymer nanocomposite samples prepared using a range of rGO concentrations was determined from the measured electrical resistivity and displayed in Fig. 8 rGO 0.2 (0.002 vol.%) and rGO 0.4 (0.004 vol.%) were not electrically conducting (i.e. insulators), which can be explained by the fact that rGO preferentially adsorbed at the original w/o interface and covers only the pore surfaces after polymerisation and drying of the poly-Pickering-HIPEs. As the rGO concentration increased to 0.8 mg/ml (corresponding to a filler content of 0.006 vol.% rGO in the macroporous polymer nanocomposite rGO 0.8), the rGO concentration was high enough to create a conductive network percolating the entire macroporous polymer as now rGO links the rGO covering pore walls through the bulk polymer forming the cell walls, resulting in a conductivity of 1.2 10^{-5} S m^{-1}. Increasing the concentration of rGO to 0.0041 vol.% (rGO 5) increased the electrical conductivity ten-fold to 1.3 10^{-4} S m^{-1}. By fitting the data points in Fig. 8 to the conductivity equation (inserted equation in Fig. 8), the percolation threshold Φ_c for rGO-poly(St-co-DVB)HIPEs was determined to be 0.005 vol.% which is about two orders of magnitude lower than the previously reported percolation threshold for dense graphene-based nanocomposites [60–62]. The low percolation threshold determined for our macroporous polymer nanocomposites could be potentially due to the location of rGO at the oil–water interface during emulsification, which resulted in an efficient arrangement of rGO particles, forming a conductive network around the pores, which are linked by rGO remaining in the polymer phase making up the final macroporous structure after polymerisation. As the rGO concentration increased, the network of rGO particles increased in density, resulting in increasing conductivity.

4. Conclusion

In this study, we utilised rGO as an emulsifier, to formulate HIPEs consisting of continuous but minority monomer (oil) phase and a dispersed aqueous electrolyte phase, which we then polymerised into conductive high porosity macroporous polymer nanocomposites. The spontaneous adsorption and organisation of rGO at the original w/o HIPE interface and the dispersion of excess rGO throughout the polymer matrix created an efficient conductive network, which gave rise to a very low percolation threshold. W/o HIPEs stabilised by a range of rGO concentrations from 0.2 mg/ml to

5 mg/ml (with respect to the organic phase volume) were prepared and polymerised at 70 °C. After polymerisation, high porosity, closed cell macroporous rGO-polymer nanocomposites were produced. The mechanical interlocking of the rGO particles within the macroporous polymer nanocomposite matrix provided increased mechanical resistance to compression. This resulted in an increase in the storage modulus by an order of magnitude just by doubling the amount of rGO from 0.4 to 0.8 mg/ml used to stabilise the HIPE templates. The maximum elastic and storage moduli determined for poly-rGO-stabilised-HIPEs were also significantly higher compared to those measured for control samples prepared by polymerising particulate and surfactant-stabilised HIPEs. The minimum percolation threshold of rGO macroporous polymer nanocomposites was determined to be 0.005 vol.% by fitting the experimentally measured resistivity to the conductivity equation. This is significantly lower than the percolation threshold determined for dense nano-composites previously reported in literature, providing evidence of the efficient arrangement of rGO within the conductive macroporous structures.

All in all, emulsion templating using rGO-stabilised HIPEs was proven to be an effective way to translate 2D rGO particles into conducting, high porosity and yet strong and stiff 3D macroporous polymer nanocomposites.

Acknowledgements

The authors would like to thank Challenging Engineering programme (EP/E007538/1) of the UK Engineering and Physical Sciences Research Council (EPSRC) and Imperial College London for funding. Eduardo Saiz and Suelen Barg acknowledge the support from the Centre for Advanced Structural Ceramics (CASC) funded by EPSRC at Imperial College London, the Leverhulme Charitable Trust Grant (Large area electronics with solution chemically derived graphene- F/07 058/BO), and the European Commission (FP7-Marie Curie Intra-European Fellowship and International Reintegration Grant:FP7-PEOPLE-2011-IEF-301909-ACIN).

Appendix A. Supplementary data

Supplementary data related to this article can be found at http://dx.doi.org/10.1016/j.polymer.2013.09.039.

References

[1] Geim AK, Novoselov KS. Nat Mater 2007;6(3):183–91.
[2] Novoselov KS, Geim AK, Morozov SV, Jiang D, Zhang Y, Dubonos SV, et al. Science 2004;306(5696):666–9.
[3] Wang X, Zhi L, Mullen K. Nano Letters 2007;8(1):323–7.
[4] Stankovich S, Dikin DA, Dommett GHB, Kohlhaas KM, Zimney EJ, Stach EA, et al. Nature 2006;442(7100):282–6.
[5] Ghosh S, Calizo I, Teweldebrhan D, Pokatilov EP, Nika DL, Balandin AA, et al. Appl Phys Lett 2008;92(15).
[6] Gómez-Navarro C, Weitz RT, Bittner AM, Scolari M, Mews A, Burghard M, et al. Nano Lett 2007;7(11):3499–503.
[7] Eda G, Fanchini G, Chhowalla M. Nat Nano 2008;3(5):270–4.
[8] Stankovich S, Dikin DA, Piner RD, Kohlhaas KA, Kleinhammes A, Jia Y, et al. Carbon 2007;45(7):1558–65.
[9] Cote LJ, Kim J, Tung VC, Luo JY, Kim F, Huang JX. Pure Appl Chem 2011;83(1):95–110.
[10] Kim J, Cote LJ, Kim F, Yuan W, Shull KR, Huang J. J Am Chem Soc 2010;132(23):8180–6.
[11] Kim F, Cote LJ, Huang JX. Adv Mater 2010;22(17):1954–8.
[12] Song X, Yang Y, Liu J, Zhao H. Langmuir 2011;27(3):1186–91.
[13] Gudarzi MM, Sharif F. Soft Matter 2011;7(7):3432–40.
[14] Sun J, Bi H. Mater Lett 2012;81(0):48–51.
[15] Guo P, Song H, Chen X. J Mater Chem 2010;20(23):4867–74.
[16] He Y, Wu F, Sun X, Li R, Guo Y, Li C, et al. ACS Appl Mater Interfaces 2013;5(11):4843–55.
[17] Mattevi C, Eda G, Agnoli S, Miller S, Mkhoyan KA, Celik O, et al. Adv Funct Mater 2009;19(16):2577–83.
[18] Bagri A, Mattevi C, Acik M, Chabal YJ, Chhowalla M, Shenoy VB. Nat Chem 2010;2(7):581–7.
[19] Dreyer DR, Park S, Bielawski CW, Ruoff RS. Chem Soc Rev 2010;39(1):228–40.
[20] Park S, An J, Jung I, Piner RD, An SJ, Li X, et al. Nano Lett 2009;9(4):1593–7.
[21] Kim H, Abdala AA, Macosko CW. Macromolecules 2010;43(16):6515–30.
[22] Yavari F, Chen Z, Thomas AV, Ren W, Cheng H-M, Koratkar N. Sci Rep 2011;1.
[23] Liang J, Huang Y, Zhang L, Wang Y, Ma Y, Guo T, et al. Adv Funct Mater 2009;19(14):2297–302.
[24] Wan D, Yang C, Lin T, Tang Y, Zhou M, Zhong Y, et al. ACS Nano 2012;6(10):9068–78.
[25] Wang H, Liang Y, Mirfakhrai T, Chen Z, Casalongue H, Dai H. Nano Res 2011;4(8):729–36.
[26] Ruiz ON, Fernando KAS, Wang B, Brown NA, Luo PG, McNamara ND, et al. ACS Nano 2011;5(10):8100–7.
[27] Ramanathan T, Abdala AA, Stankovich S, Dikin DA, Herrera Alonso M, Piner RD, et al. Nat Nano 2008;3(6):327–31.
[28] Xu Y, Hong W, Bai H, Li C, Shi G. Carbon 2009;47(15):3538–43.
[29] Zhang H-B, Yan Q, Zheng W-G, He Z, Yu Z-Z. Acs Appl Mater Interfaces 2011;3(3):918–24.
[30] Chen ZP, Ren WC, Gao LB, Liu BL, Pei SF, Cheng HM. Nat Mater 2011;10(6):424–8.
[31] Verdejo R, Barroso-Bujans F, Rodriguez-Perez MA, Antonio de Saja J, Lopez-Manchado MA. J Mater Chem 2008;18(19):2221–6.
[32] Vickery JL, Patil AJ, Mann S. Adv Mater 2009;21(21):2180–4.
[33] Niu Z, Chen J, Hng HH, Ma J, Chen X. Adv Mater 2012;24(30):4144–50.
[34] Delle LE, Lanche R, Law JK-Y, Weil M, Vu XT, Wagner P, et al. Physica Status Solidi (A) 2013;210(5):975–82.
[35] Cameron NR. Polymer 2005;46(5):1439–49.
[36] Barbetta A, Carnachan RJ, Smith KH, Zhao C-T, Cameron NR, Kataky R, et al. Macromol Symp 2005;226(1):203–12.
[37] Cameron N, Sherrington D, Albiston L, Gregory D. Colloid Polym Sci 1996;274(6):592–5.
[38] Lissant KJ. J Colloid Interface Sci 1966;22(5):462–8.
[39] Moglia RS, Holm JL, Sears NA, Wilson CJ, Harrison DM, Cosgriff-Hernandez E. Biomacromolecules 2011;12(10):3621–8.
[40] Wong LLC, Ikem VO, Menner A, Bismarck A. Macromol Rapid Commun 2011;32(19):1563–8.
[41] Zhao C, Danish E, Cameron NR, Kataky R. J Mater Chem 2007;17(23):2446–53.
[42] Cameron N, Sherrington D. High internal phase emulsions (HIPEs)—structure, properties and use in polymer preparationIn Biopolymers liquid crystalline polymers phase emulsion. Springer; 1996. p. 163–214.
[43] Menner A, Ikem V, Salgueiro M, Shaffer MS, Bismarck A. Chem Commun (Camb) 2007;41:4274–6.
[44] Wu R, Menner A, Bismarck A. Polymer 2013;54:5511–7.
[45] Aveyard R, Binks BP, Clint JH. Adv Colloid Interface Sci 2003;100–102(0):503–46.
[46] Binks BP, Lumsdon SO. Langmuir 2001;17(15):4540–7.
[47] Yang YL, Gupta MC. Nano Lett 2005;5(11):2131–4.
[48] Menner A, Verdejo R, Shaffer M, Bismarck A. Langmuir 2007;23(5):2398–403.
[49] Claire Hermant M, Klumperman B, Koning CE. Chem Commun 2009;19:2738–40.
[50] Ikem VO, Menner A, Bismarck A. Soft Matter 2011;7(14):6571–7.
[51] Ikem VO, Menner A, Horozov TS, Bismarck A. Adv Mater 2010;22(32):3588–92.
[52] Hirata M, Gotou T, Horiuchi S, Fujiwara M, Ohba M. Carbon 2004;42(14):2929–37.
[53] Manley SS, Graeber N, Grof Z, Menner A, Hewitt GF, Stepanek F, et al. Soft Matter 2009;5(23):4780–7.
[54] Shih C-J, Lin S, Sharma R, Strano MS, Blankschtein D. Langmuir 2011;28(1):235–41.
[55] Li XL, Zhang GY, Bai XD, Sun XM, Wang XR, Wang E, et al. Nature Nanotechnol 2008;3(9):538–42.
[56] Yang D, Velamakanni A, Bozoklu G, Park S, Stoller M, Piner RD, et al. Carbon 2009;47(1):145–52.
[57] Ikem VO, Menner A, Bismarck A. Angewandte Chemie Int Ed 2008;47(43):8277–9.
[58] Wong LLC, Baiz Villafranca PM, Menner A, Bismarck A. Langmuir 2013;29(20):5952–61.
[59] McLachlan DS, Chiteme C, Park C, Wise KE, Lowther SE, Lillehei PT, et al. J Polym Sci Part B Polym Phys 2005;43(22):3273–87.
[60] Pang H, Chen T, Zhang G, Zeng B, Li Z-M. Mater Lett 2010;64(20):2226–9.
[61] Tkalya E, Ghislandi M, Alekseev A, Koning C, Loos J. J Mater Chem 2010;20(15):3035–9.
[62] Potts JR, Dreyer DR, Bielawski CW, Ruoff RS. Polymer 2011;52(1):5–25.